Nuclear Instruments and Methods in Physics Research B 267 (2009) 3624–3632

Contents lists available at ScienceDirect

Nuclear Instruments and Methods in Physics Research B

journal homepage: www.elsevier.com/locate/nimb

Incorporation of the Goudsmit–Saunderson electron transport theory in the Geant4 Monte Carlo code

O. Kadri [a,*], V. Ivanchenko [b,c], F. Gharbi [a], A. Trabelsi [a]

[a] National Center for Nuclear Sciences and Technologies, 2020 Tunis, Tunisia
[b] CERN, CH-1211 Geneve 23, Switzerland
[c] Ecoanalytica, Moscow State University, Moscow, Russia

ARTICLE INFO

Article history:
Received 12 May 2009
Received in revised form 14 September 2009
Available online 17 September 2009

PACS:
34.80.Bm
07.05.Tp
02.70.Ss
02.50.Ng

Keywords:
GEANT4
Multiple elastic scattering
Goudsmit–Saunderson theory

ABSTRACT

The present work describes the implementation of the multiple scattering formalism for charged particle transport based on the Goudsmit–Saunderson angular distribution and satisfying the Lewis spatial displacement theories. Furthermore, the most realistic total cross sections and transport cross sections for single elastic scattering of electrons and positrons by neutral atoms were carried out using the ELSEPA code. The extended model has been incorporated in the Geant4 Monte Carlo code system (currently used in many fields of application for transport of particles and covering a large range of energies from 0.1 keV to 100 TeV). Additionally, techniques are developed that allow the distributions to be scaled to account for energy loss. This new representation allows on-the-fly sampling of Goudsmit–Saunderson angular distributions in a screened Rutherford approximation suitable for Class II condensed history Monte Carlo codes. The reliability of the model is demonstrated through a comparison of simulation results with experimental data. Good agreement is found for electrons with kinetic energies down to a few keV.

1. Introduction

This paper is concerned with the theoretical description and Monte Carlo simulation of elastic scattering of fast charged particles, especially electron and positron, in matter. Modelling electron transport by Monte Carlo method is an involved process. A realistic model must account for the effects of elastic scattering by atomic nuclei, inelastic scattering by atomic electrons, production of delta-rays and production of bremsstrahlung. However, the main complication of the event-by-event ("detailed") simulation is the large number of interactions suffered by an electron in the course of its slowing down, which becomes impractical for most of the electron energy range of interest in radiation processing, radiation shielding, medical applications and astrophysics (say a few hundred eV to few TeV). The "condensed history" approach to electron transport (see [1]) overcomes this complication. Such approach simulates the change in energy, direction and position of electron (of course charged particles in general) along their trajectories by studying the global effect of the multiple interactions suffered by an electron along a trajectory segment of a given length [1].

The last scheme have been adopted in many high energy Monte Carlo simulation codes such as ETRAN [2], ITS3 [3], MCNP [4], EGS4 [5], EGSNRC [6], Geant3 [7], and Geant4 [8] with the help of the most commonly used theories of Williams [9], Molière [10], Lewis [11] and Goudsmit–Saunderson [12]. The multiple scattering model used in Geant4 is based on the Lewis' theory and a modified Highland formula for the angular distributions [13].

In the present paper, we incorporate a multiple elastic scattering of electron model based on Goudsmit–Saunderson angular distribution and Lewis spatial displacement. In principle, the angular deflections are sampled from tabulated distributions (probability density function (PDF) and their cumulative (CPDF)) for pre-selected step lengths. Furthermore, the space displacements are generated by means of the algorithm proposed by Kawrakow et al. [14], which is accurate to fourth order to imitate Lewis displacement moments. The total cross sections and the transport elastic cross sections for electron and positron covering the wide energy range of 100 eV to 1 GeV and the target atomic number of 1–103 were generated using the ELSEPA [15] code and therefore included as a separate data base. In addition to the path length and the particle energy, the third parameter needed for the angular sampling, which is the screening parameter, was adjusted in such a way to reproduce the correct cross sections from the screened Rutherford single scattering cross section.

* Corresponding author. Address: National Center for Nuclear Sciences and Technologies, 2020 Tunis, Tunisia. Tel.: +216 21493773; fax: +216 71537555.
E-mail address: omrane.kadri@cnstn.rnrt.tn (O. Kadri).

0168-583X/$ - see front matter © 2009 Elsevier B.V. All rights reserved.
doi:10.1016/j.nimb.2009.09.015

In Section 2, theoretical models adopted to accurately compute space-angular distributions for charged particle, especially electron, scattering are briefly reviewed. The complete simulation algorithm is described in Section 3, where we discuss the practical implementation of the "on-the-fly" sampling of Goudsmit–Saunderson angular distributions and the computation of different required cross sections. Numerical results, showing the accuracy attainable with this kind of algorithm, are presented in Section 4.

2. Electron transport theory

The theory of elastic and inelastic scattering of charged particles from atoms has been presented in a number of studies during the last century. We present order of magnitude estimates for the elastic scattering of an unpolarized electron from a neutral atom at any incident velocity (relativistic or non relativistic). Here we review only enough to remind the reader of the basic theory and to make understandable the magnitude of numerical data based on much more careful calculations, followed to construct the proposed algorithm. We consider an electron (or positron) with kinetic energy E starting off at the origin of the laboratory frame, and moving in the direction of the z-axis in a hypothetical infinite homogeneous medium, with N scattering centers (spherically symmetrical atoms or randomly oriented molecules) per unit volume. The single scattering differential cross section (DCS) is assumed to be symmetric about the incident direction (z-axis), i.e. depends only on the polar angle θ. For simplicity, we limit our considerations to single-element targets.

2.1. Angular distribution

It is well known that the Goudsmit–Saunderson theory gives an accurate description of the angular distribution of particles which have traveled a path length s (total path length in units of mean free path). For that, the above scheme was chosen and here we will, briefly, present all necessary formula. The angular distribution, $f_1(\theta)$, after a single elastic scattering event, is given by

$$f_1(\theta) = \frac{1}{\sigma}\frac{d\sigma(\theta)}{d\Omega} \tag{1}$$

where, $d\sigma/d\Omega$ is the DCS and σ is the total elastic cross section

$$\sigma = \int \frac{d\sigma(\theta)}{d\mu} d\mu \tag{2}$$

where $\mu = (1-\cos(\theta))/2$, the reduced cosine polar angle which varies from 0 (forward scattering) to 1 (backscattering).

The mean free path, lambda, between elastic collisions is given by

$$\lambda = \frac{1}{N\sigma} \tag{3}$$

where $N = \rho N_0/A$ (N_0, ρ and A are Avogadro's number, the density and the atomic weight of the medium, respectively) is the number of atoms per unit volume.

The normalized multiple scattering distributions has the form of a Legendre series expansion

$$F_{GS}(\theta, s) = \sum_{l=0}^{\infty}(l+1/2)\mathrm{e}^{-sQ_l}P_l(\cos(\theta)) \tag{4}$$

where Q_l denotes the moments of the single scattering distribution.

For the screened Rutherford cross section, the work of Kawrakow et al. [16] found a stable expression of Q_l:

$$Q_l = 1 - yK_1(y)\left\{1 + 0.5y^2\left\{1 + \frac{1}{2} + \cdots + \frac{1}{l} - 0.5\ln(l(l+1)) - 0.5772\right\}\right\} \tag{5}$$

K_1: The modified Bessel function, A the screening parameter and $y = 2\sqrt{l(l+1)A}$. At high energies and relatively large scattering angles, the incident electron scatters from the nucleus by Coulomb scattering. Screening by the atomic electrons affects scattering only at small angles when the electron passes at a large impact parameter. At lower energies, screening is important even at large scattering angles.

The number of terms required to reach the convergence of the Legendre expansion series increases as the path length becomes shorter, particularly for large scattering angles. We have used up to 1000 Q_l moments to achieve the convergence of that series.

The convergence of the expansion series in the case of small path lengths can be improved by separating the contributions of electrons without collision from sum series, yielding to:

$$F_{GS}(\theta, s) = \mathrm{e}^{-s}\delta(1-\cos(\theta)) + \sum_{l=0}^{\infty}(l+1/2)(\mathrm{e}^{-sQ_l} - \mathrm{e}^{-s})P_l(\cos(\theta)) \tag{6}$$

Fig. 1 shows the probabilities of no, single and two or more collisions vs. mean free paths number (s), as suggested by Berger [1] in rewriting the Goudsmit–Saunderson distribution on the following formula:

$$F_{GS}(\theta, s) = \mathrm{e}^{-s}\delta(1-\cos(\theta)) + s\mathrm{e}^{-s}f_1(\theta) + (1-s-s\mathrm{e}^{-s}) \times \sum_{l=0}^{\infty}(l+1/2)\frac{\mathrm{e}^{-sQ_l} - [1+s(1-Q_l)]\mathrm{e}^{-s}}{1-(1+s)\mathrm{e}^{-s}}P_l(\cos(\theta)) \tag{7}$$

As it is shown, above about 12 mean free paths, only the multiple scattering regime exists.

2.2. Spatial displacement

Every condensed history Monte Carlo code system uses its own scheme to correlate between final direction and position of the electron after multiple scattering process. From literature the most accurate and commonly followed way that's described by Lewis [11] is giving, essentially, five space-angular moments.

The algorithm proposed uses the averaged relation formula given by Bielajew et al. [17]. Neglecting the energy loss during the history of the particle's track, these equations are given by:

$$\frac{\langle z\rangle}{s} = \frac{1-\mathrm{e}^{-\xi}}{\xi} \tag{8}$$

$$\frac{\langle z\mu\rangle}{s} = \frac{1}{3\xi}\left(1 - \mathrm{e}^{-\xi} + 2\frac{\mathrm{e}^{-\xi} - \mathrm{e}^{-\gamma\xi}}{\gamma-1}\right) \tag{9}$$

$$\frac{\langle x\sin\Theta\cos\Phi + y\sin\Theta\sin\Phi\rangle}{s} = \frac{2}{3\xi}\left(1 + \frac{\mathrm{e}^{-\gamma\xi} - \gamma\mathrm{e}^{-\xi}}{\gamma-1}\right) \tag{10}$$

$$\frac{\langle z^2\rangle}{s^2} = \frac{2}{3\gamma\xi^2}\left(\gamma(\xi + \mathrm{e}^{-\xi}) - (\gamma-2) + 2\frac{\mathrm{e}^{-\gamma\xi} - \gamma\mathrm{e}^{-\xi}}{\gamma-1}\right) \tag{11}$$

$$\frac{\langle x^2+y^2\rangle}{s^2} = \frac{4}{3\gamma\xi^2}\left(\gamma\xi - (\gamma+1) - \frac{\mathrm{e}^{-\gamma\xi} - \gamma^2\mathrm{e}^{-\xi}}{\gamma-1}\right) \tag{12}$$

where (x, y, z) are the laboratory coordinates of the particle having scattered by (Θ, Φ) as polar and azimuthal deflections respectively. Within our considerations Θ results from the Goudsmit–Saunderson distribution and Φ uniformly distributed between 0 and π.

For the spatial displacement, the two coefficient keys $\xi = sQ_1$ and $\gamma = Q_2/Q_1$ spans the ranges of (0–1) and (0–3), respectively. The backscattering is characterized by $\gamma = 0$, whereas, γ tends to three for the forward scattering and/or high energy regime.

We adopted "the best solution found" by Kawrakow et al. [14] to satisfy the Lewis moments, which consists on splitting each step into two equally spaced sub-steps.

If we consider (θ_1, ϕ_1) and (θ_2, ϕ_2) as the two couples of scattering angles for the two sub-steps, the final momentum cosine directions becomes:

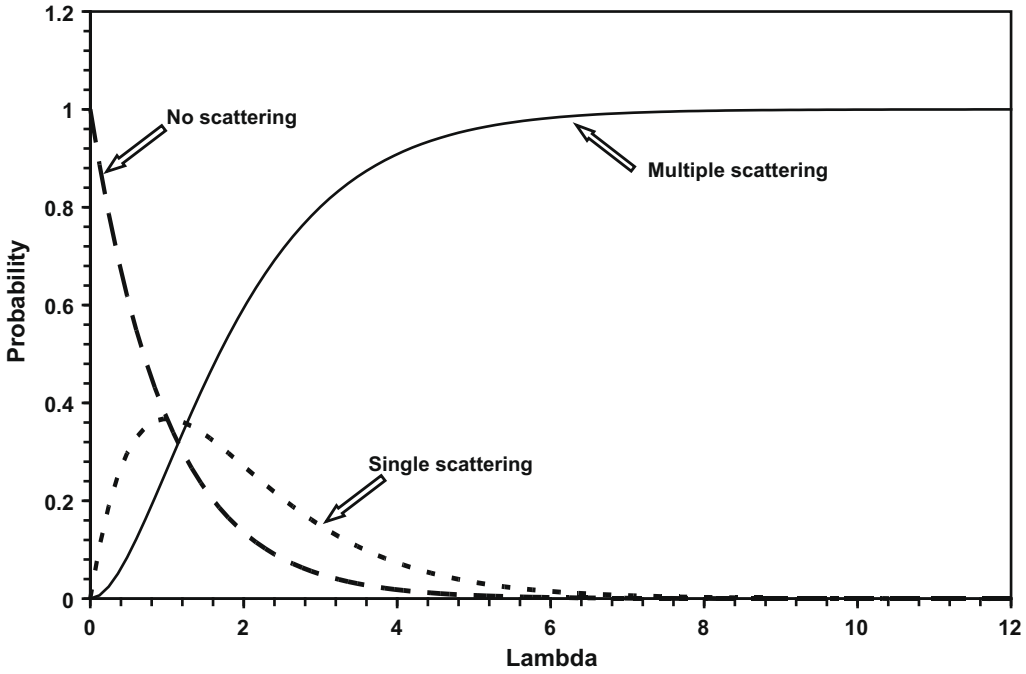

Fig. 1. Probability distributions vs. path length in terms of mean free paths (Lambda) of: no scattering (long dashed), single scattering (short dashed) and multiple scattering (curve).

$$v_x = \sin\theta_2(\cos\theta_1\cos\phi_1\cos\phi_2 - \sin\phi_1\sin\phi_2) + \cos\theta_2\sin\theta_1\cos\phi_1 \quad (13)$$

$$v_y = \sin\theta_2(\cos\theta_1\sin\phi_1\cos\phi_2 + \cos\phi_1\sin\phi_2) + \cos\theta_2\sin\theta_1\sin\phi_1 \quad (14)$$

$$v_z = \cos\theta_1\cos\theta_2 - \sin\theta_1\sin\theta_2\cos\phi_2 \quad (15)$$

and the final Cartesian coordinates:

$$x/s = \eta_1\sin\theta_1\cos\phi_1 + \eta_2\sin\theta_2(\cos\phi_1\cos\phi_2 - \cos\theta_1\sin\phi_1\sin\phi_2) + \eta_0 v_x \quad (16)$$

$$y/s = \eta_1\sin\theta_1\sin\phi_1 + \eta_2\sin\theta_2(\sin\phi_1\cos\phi_2 + \cos\theta_1\cos\phi_1\sin\phi_2) + \eta_0 v_y \quad (17)$$

$$z/s = \eta_0 + \eta_1\cos\theta_1 + \eta_2\cos\theta_2 + \eta_0 v_z \quad (18)$$

where η_0, η_1 and η_2 are adjustable parameters.

2.3. Accounting for energy loss

Due to the path length dependence on the particle's energy, the DCSs depend also on the energy. To take into account the energy loss during the history of the electron track which is not done explicitly within the Q_l moments, we use the following effective energy (E_1) and path length (s_1), based on [6]:

$$E_1 = E\left[1 - \epsilon^2\frac{(6+10\tau+5\tau^2)}{(24\tau^2+48\tau+72)}\right] \quad (19)$$

$$s_1 = s\left(1 - \frac{\epsilon^2}{3(2-\epsilon)}\frac{4+6\tau+7\tau^2+4\tau^3+\tau^4}{(\tau+1)^2(\tau+2)^2}\right) \quad (20)$$

where $\tau = (E - 0.5\Delta E)/mc^2$, $\epsilon = \Delta E/E$, for a given energy loss, ΔE, during the path-length s and mc^2 the particle's rest mass energy.

3. Model implementation in Geant4

Before invoking the simulation algorithm as proposed, we describe in the following the cross sections used and the pre-calculated angular distributions data bases, as well as the necessary path-length-correction imposed by geometrical–physical constraints.

3.1. Cross sections data base

Generally, Monte Carlo code systems use approximate analytical formula to compute the total elastic cross sections and the transport cross sections (unscreened Rutherford, screened Rutherford, Mott's scheme etc ...) to simulate charged particles scattering. The current model used a most realistic data base generated by ELSEPA code [15].

The present database for elastic scattering of electrons and positrons by atoms has been calculated by using the Dirac partial-wave-expansion method with interaction potentials obtained from the static-field approximation. Data are provided for the elements, $Z = 1$–103, and for a grid of kinetic energies spanning the interval from 100 eV up to 1 GeV. The calculations have been performed by means of the ELSEPA code. For each element 106 kinetic energy points were chosen to cover the possibly reached interval. Cubic spline method, for a given Z, has been adopted to accurately interpolate cross sections between data. Whereas, for energies up to 100 TeV a log–log extrapolation is used for both electron and positron particles. Notice that the calculations for compound materials were straightforward done using the additivity rule (addition by atomic weight).

Fig. 2 shows a good agreement between the Urban (currently adopted model in Geant4) computations of transport cross sections as function of electron kinetic energy and those generated from the data base for low-Z (Aluminum) and for high-Z (Lead).

3.2. Pre-calculated angular deflections

Pre-calculated angular deflections, correctly computed, lead to sophisticated Monte Carlo simulation methods.

To achieve a good accuracy, we calculated the PDF's and their CPDF's for a given path length, screening angle and a given random number, in a dense grid of 16 subdivisions per decade in the path

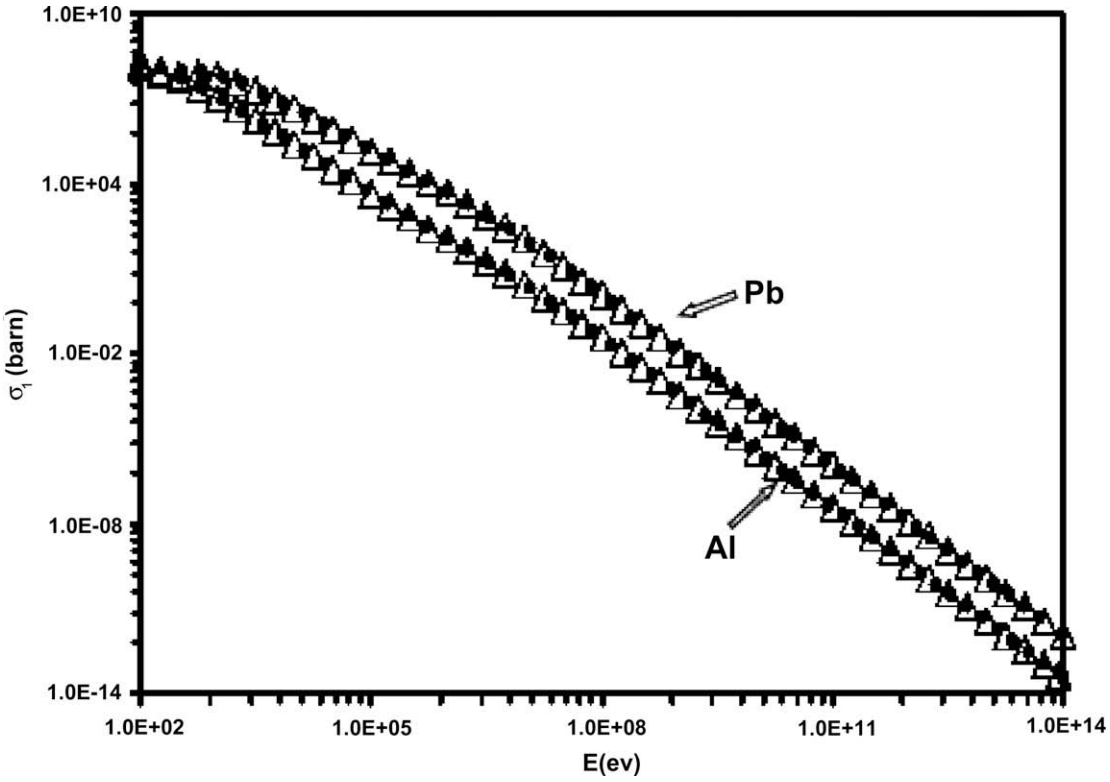

Fig. 2. Transport cross section σ_1 in barn vs. kinetic energy E in eV distributions for Al and Pb materials: empty circles and diamonds represent the Urban calculations and filled squares and triangles represent the current work calculations.

length (s) direction and covering the range of $1–10^5$. Since the "detailed" simulation is computationally feasible only when the average number of events along an electron track is relatively small, we limit our calculations to the case of path length's equal to one mean free path. For each s value, 11 dynamic screening parameters are used allowing to spans the range of 0.001–0.5 values of $Q_1' = sQ_1$. In fact, Q_1' varies from 0 to higher than 0.5 (multiple scattering upper acceptable limit), so, the two other intervals (0–0.001) and (>0.5) will be treated separately in the "Algorithm" subsection, in order to optimize the allowed memory for the data base.

For each couple (s,A), the reduced angle range is subdivided into 320 values between 0 and 1 with a higher density near 0 enough to well predict forward scatterings (most probable events).

For the multiple scattering angular sampling on run-time, fast and accurate interpolation procedure between the corresponding

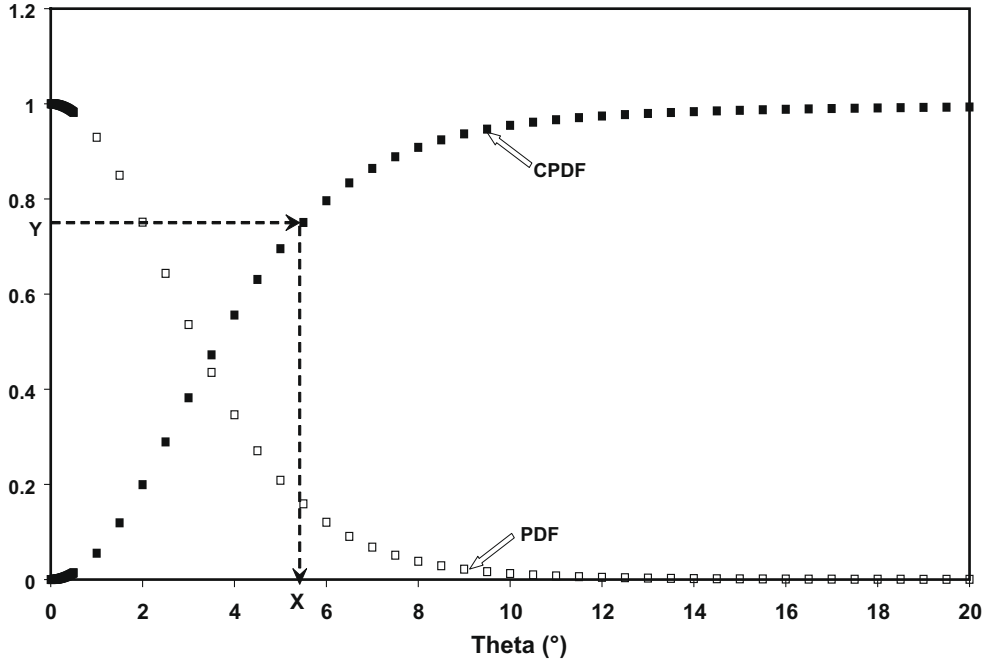

Fig. 3. Illustrative example of the inverse cumulative sampling method (PDF and CPDF are arbitrary calculated for a given couple (s,A)).

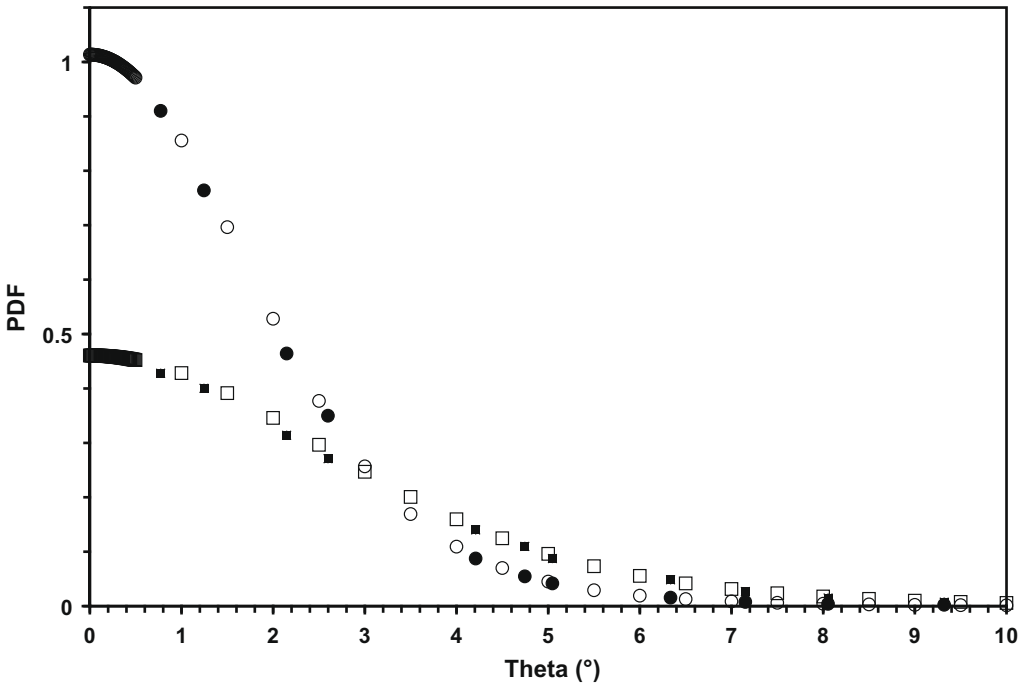

Fig. 4. Normalized PDF distributions for 15.7 MeV kinetic energy electron beams impinging normally on gold slabs. Empty circle and square represent Hanson data for 9 and 19 μm Au thickness, respectively. Filled circle and square represent the current calculations for 9 and 19 μm Au thickness, respectively. Curve with PDF unity at 0° correspond for the 9 μm case.

PDF and CPDF for a given path length, screening angle and a given random number (s, A, μ). This is done following the Benedito's procedure. Which is described elsewhere [18] and essentially used the inverse cumulative sampling technique, i.e. by the Newton iterative method, for example, we can sample $x = \cos(\theta)$ from CPDF$(x) - y = 0$, where y is a uniformly generated random number.

An illustrative example for the inverse cumulative sampling technique is shown in the Fig. 3.

Fig. 4 shows a comparison between calculated and measured [19] PDF's of electron beams having a kinetic energy of 15.7 MeV normally incident on thin slabs of gold (about 19 μm and 9 μm thickness). A satisfactory agreement is seen at least until this stage of the implementation description.

3.3. Path length correction

From the Urban [13] multiple scattering model used by Geant4, we adopted, for our proposed model, the same path length correction (or transformations) strategy.

Keeping in mind that the true path length t which is the total length traversed by a particle is restricted (checks should be done to take the minimum proposed step) by all possible physical processes. Furthermore, the geometrical path length g which is the minimal distance between initial and final step points (straight line for non magnetic field) is restricted by experimental geometries and thus boundaries.

By path length transformations, it means the restriction of the step length twice, one time by physical processes and the other time by geometrical setup.

A more elaborate and detailed description of that correction was proposed by Urban [13].

3.4. Algorithm

Assembling all these pieces we found a powerful algorithm to simulate elastic scattering process, which is incorporated in Geant4 toolkit written in C++ language, by writing two classes "G4GoudsmitSaundersonMscModel" and "G4GoudsmitSaundersonTable". These classes called in run-time the cross section's and the PDF's separately constructed data bases.

The practical implementation of the algorithm to generate random electron tracks is as follows, assuming that the electron starts with a kinetic energy E and moving along the z-axis:

(i) Using the elastic scattering cross sections and the path length transformations, the true path length in terms of the mean free path is given.
(ii) Take into account the energy loss (Eq. (18) + Eq. (19)).
(iii) From the Goudsmit–Saunderson distributions sample two couples of polar and azimuthal scattering angles (θ_1, ϕ_1) and (θ_2, ϕ_2) for the two equally spaced virtual sub-steps following this procedure for each theta and randomly shooting the azimuthal angle between 0 and 2π:
  (1) generate a uniform random number r,
  (2) if $r < e^{-s}$: corresponding to the no scattering case; then the reduced angle $\mu = 0$,
  (3) else, if $r < (1+s)e^{-s}$:the single scattering case; sample theta from the screened Rutherford distribution, i.e. $\mu = rA/(1-r+A)$,
  (4) else: the multiple scattering case;
    (a) if $s < 1$ or $sQ_1 < 0.001$: plural or small angle scattering case; sample theta with the procedure described by Bielajew [20],
    (b) else if $sQ_1 > 0.5$: isotropic distribution case; randomly sample theta between 0 and π,
    (c) else: sample theta using the inverse cumulative method, i.e. for a given (s, A, r) we search μ from lookup tables (PDF's data base),
  (5) change the momentum direction by rotating the cosine directions (Eqs. (12)–(14)) around the old momentum direction taken as z-axis,
  (6) finally, let the particle advance to the final position given by its Cartesian coordinates (Eqs. (15)–(17)).

4. Model validation

In using electron beams for industrial processing, radiation shielding and medical treatment, as well for basic research, it is important to have accurate knowledge of the transport of particles through matter details. Such knowledge includes lateral and longitudinal displacement, transmission, reflection and absorption coefficient numbers and depth-dose profiles also.

In the following some benchmarks were presented to demonstrate the quality of the new transport mechanics algorithm described above.

4.1. Lateral and longitudinal displacement

We performed simulations of spatial (lateral and longitudinal) distributions of electrons with various energies after traversing

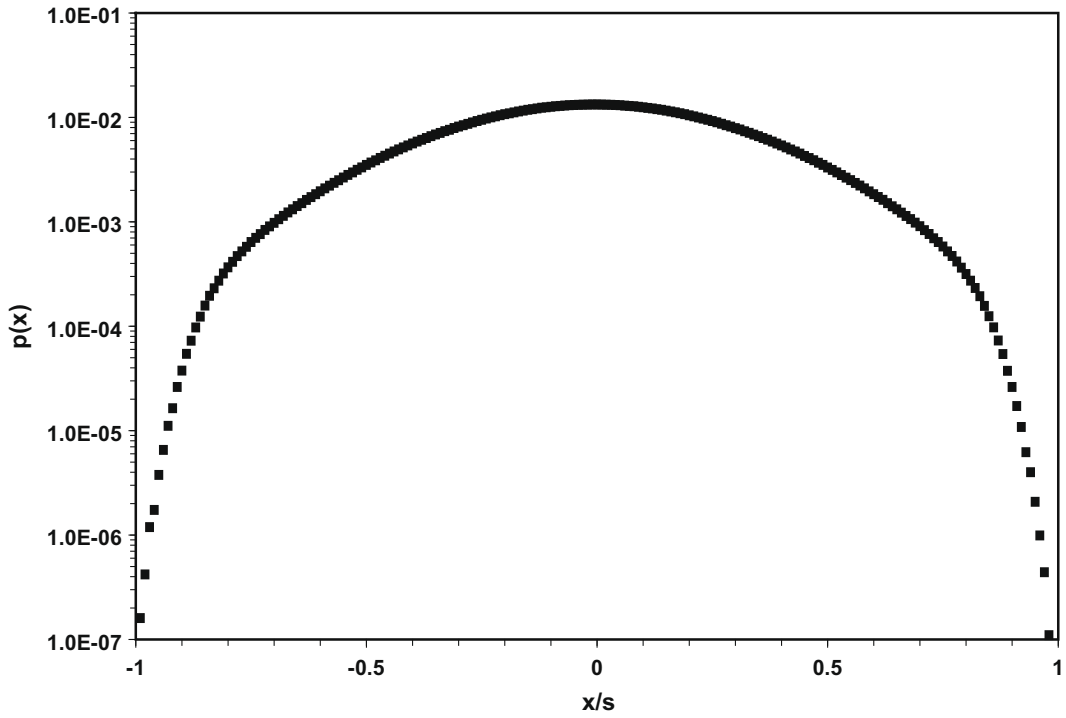

Fig. 5. Multiple-scattering projected transverse displacement (x coordinate) distribution $p(x)$ of 100 keV electrons after traversing 75 mean free paths in an infinite Pb medium.

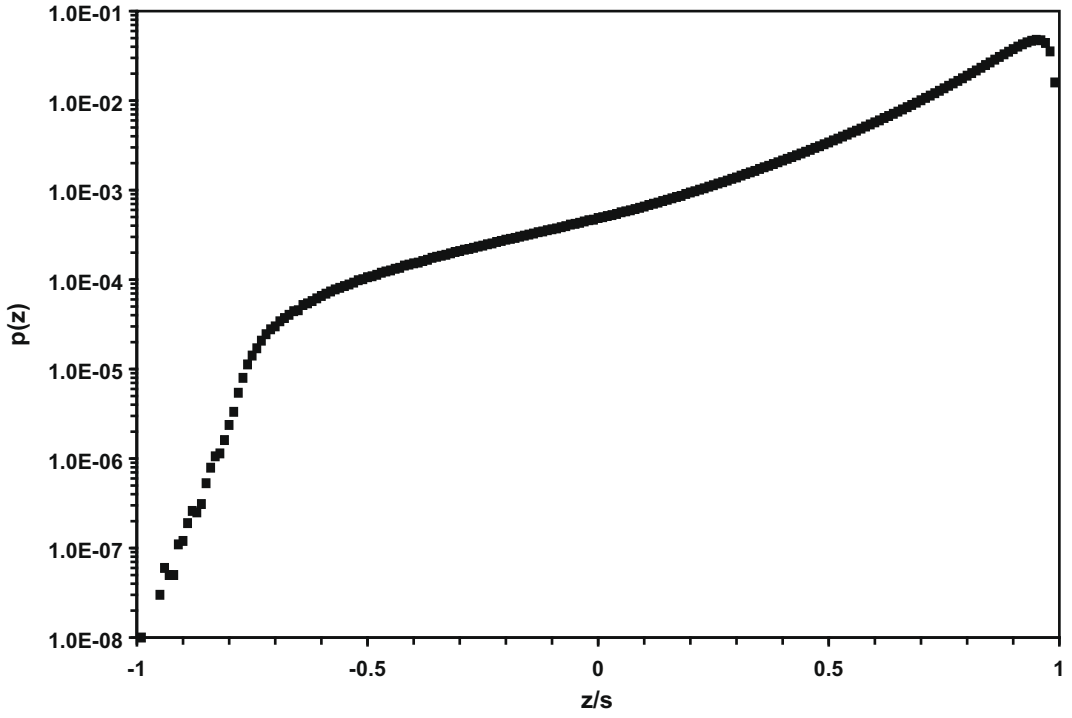

Fig. 6. Multiple-scattering longitudinal displacement distribution $p(z)$ of 100 keV electrons after traversing 75 mean free paths in an infinite Pb medium.

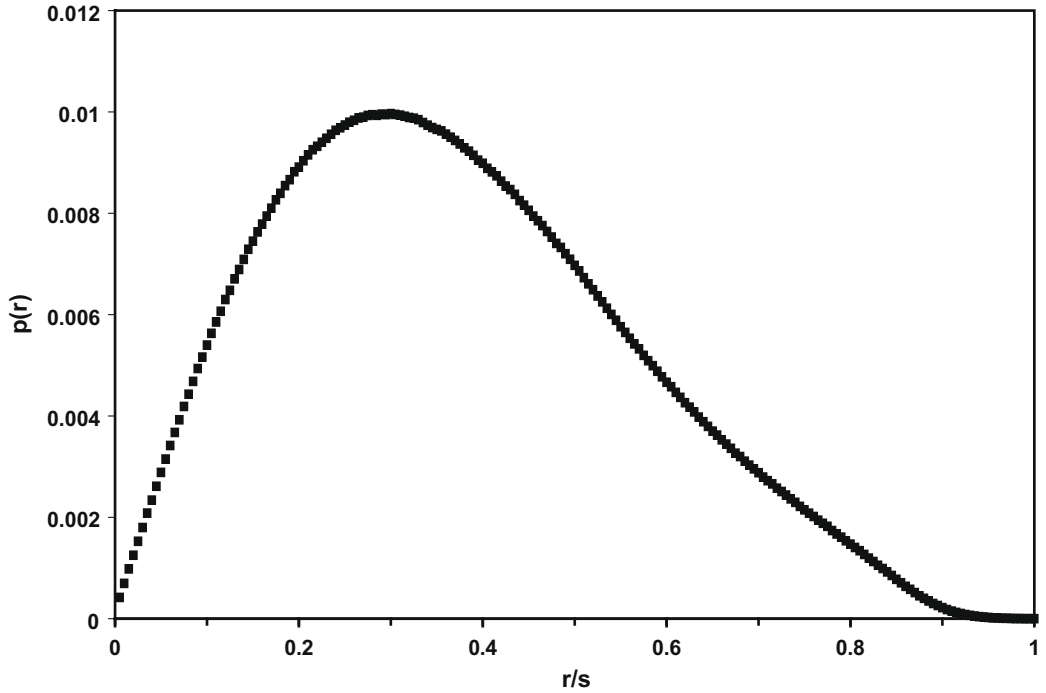

Fig. 7. Multiple-scattering lateral displacement distribution of 100 keV electrons after traversing 75 mean free paths in an infinite Pb medium.

Table 1
Benchmarks against Seltzer data: S: Seltzer data; T: this work; TN (RN), transmission (reflection) coefficient number; TE (RE), transmission (reflection) energy coefficient; PhiA, energy absorption coefficient. Cases of electrons with kinetic energy of 100, 150, 200, 300 and 400 keV normally incident on slabs of Al and Ti.

	Param	100		150		200		300		400	
		S	T	S	T	S	T	S	T	S	T
Al	TN	0.602	0.607	0.918	0.924	0.968	0.980	0.997	1.001	1.004	1.006
	TE	0.393	0.403	0.766	0.772	0.880	0.883	0.949	0.949	0.969	0.968
	RN	0.124	0.126	0.070	0.075	0.031	0.037	0.010	0.011	0.005	0.005
	RE	0.071	0.072	0.045	0.046	0.022	0.025	0.007	0.007	0.002	0.003
	PhiA	0.536	0.532	0.189	0.188	0.098	0.096	0.044	0.045	0.029	0.029
Ti	TN	0.105	0.082	0.597	0.565	0.808	0.812	0.957	0.969	0.985	0.996
	TE	0.050	0.039	0.419	0.394	0.662	0.660	0.873	0.878	0.931	0.936
	RN	0.224	0.186	0.213	0.209	0.161	0.168	0.053	0.054	0.024	0.024
	RE	0.142	0.118	0.133	0.129	0.107	0.111	0.039	0.040	0.018	0.018
	PhiA	0.808	0.847	0.448	0.489	0.231	0.243	0.088	0.089	0.051	0.051

different path lengths in a number of elements. However, here we will only present the graphical results for 100 keV electrons in Pb with path lengths of 75 mean free paths (MFPs). This corresponds to $\gamma = 2.185$ and $\xi = 0.507$.

For the same purpose, Figs. 5–7 show a good agreement with a previously work done by Bielajew et al. [17].

4.2. Transmission, reflection and absorption coefficient number

A transmission, absorption and backscattering experiment, similar to those described in Ref. [21], is used as a test case.

A collimated electron beams with energies between 100 keV and 400 keV impinges normally on the anterior surface of an aluminum or a titanium foil of 1 mil (1 mil = 0.001 inch = 25.4 μm) thickness.

Table 1 illustrates simulation results, using the incorporated model, and the Seltzer's data including transmission and reflection coefficients (for particle number) and the fraction of the energy absorbed in the foil of electrons. The good agreement is seen and a correct use of the model, at least within this kind of applications, is achieved. The cutoff energy of electrons and photons is taken to be 990 eV. Notice that the number of primary particles was 100,000 and the resulting statistical errors on the computed coefficients do not exceed 2% at overall energies whereas data uncertainties can be found in Ref. [21].

4.3. Depth-dose profile

As a final test for this study, absolute electron dose measurements carried out at the Sandia laboratories [23] are compared with the results of Monte Carlo simulations performed by the Geant4 code system including the proposed model. A detailed description of the calorimetric method (calorimetric response theory, experimental design, data analysis, and calibration) can be found in the Ref. [23] or [22]. Seeing that the multiple scattering causes the increase of the average path length within a constant increment of depth and thus the increase of energy deposition with increasing depth, this test comes with a special importance for the current benchmark purposes.

In this study, the depth dose distribution (deposited energy per unit depth) for 0.521 MeV electron beams normally incident on Aluminum media of about 1 mm thickness are compared with

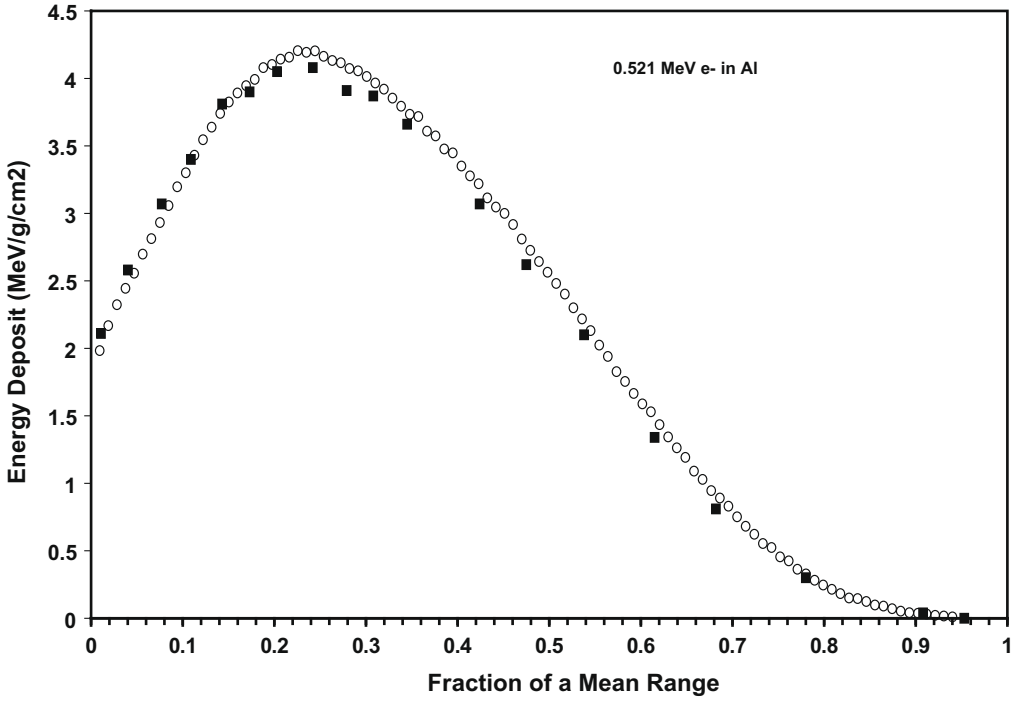

Fig. 8. Depth dose profile for 0.521 MeV electrons normally incident on an Aluminum foil. Circles and filled squares represent the simulation results and the Sandia data, respectively.

experimental data. The primary and secondary electrons are transported down to a kinetic energy of about 1 keV and bremsstrahlung photons are generated above the threshold energy of 1 keV.

The relevant depth dose distributions are calculated as a function of the scaled depth in terms of Fraction of a Mean Range (FMR).It is shown that by expressing foil thicknesses in units of.the electron range one can "scale" the data, thereby reducing the explicit dependence on the beam energy and facilitating interpolation with respect to energy and foil thickness.

The number of particles generated is changed until the statistical uncertainty of the simulations is of the order of 1% of the dose maximum. The simulated and measured distributions are, overall, reasonably close to each other within the combined computational and experimental uncertainties.

5. Conclusions

We have described a robust algorithm for the numerical calculation of multiple scattering angular distributions providing realistic spatial-angular correlations of charged particles after traversing a given path-length in the medium to high energy range. The implementation of this algorithm has been described in detail and the accuracy of the calculated results has been assessed by comparison with available experimental data.

A pre-calculated numerical representation of the Goudsmit–Saunderson multiple-scattering distribution for preselected path-lengths has been calculated using the ELSEPA total elastic cross sections and first transport cross sections with a screening parameter adjusted to reproduce the screened Rutherford ones. Using the Kawrakow's schema to describe the spatial displacement by splitting each step into two sub-steps, the energy loss effects were taken into account and the Lewis moments were reproduced, so the spatial-angular correlations were well fulfilled using the current developed model.

The database represents the scattering distribution over a range of mean free paths from 1 to 10^5, screening parameters covering a wide dynamic range and all scattering angles between 0 and π.

An electron transport benchmark study was performed in this framework to examine some parameters such as: lateral and longitudinal displacement, transmission, reflection and absorption coefficient numbers and depth-dose profile. The simulated and measured distributions are, overall, reasonably close to each other within the combined computational and experimental uncertainties (see Fig. 8).

The tests carried out with Geant4 code show that the new transport algorithm is a powerful tool for extending the capabilities and a substantial improvement of such code also. Although more extensive tests are needed for an ultimate assessment on the validity of the model, the presented comparisons are very hopeful.

Acknowledgments

We would like to express our gratitude to Prof. Iwan Kawrakow for enlightening discussions, Prof. Francesc Salvat for sending a copy of the ELSEPA code and Prof. T. Nakatsuka also. Additionally, we wish to thank all the Geant4 Team, epsecially John Apostolkalis, Michel Maire, Laszlo Urban, Alexander Bagulya and Gabriele Cosmo for the useful discussions and help in releasing of the described model with the Geant4 toolkit.

References

[1] M.J. Berger, Methods in Comput. Phys., vol. 1, Academic Press, New York, 1963. p. 135.
[2] S.M. Seltzer, in: T.M. Jenkins et al. (Eds.), Monte Carlo Transport of Electrons and Photons, Plenum Press, New York, 1988, pp. 153–181.
[3] J.A. Halbleib et al., Sandia Report Sand91-1634, 1992.
[4] J.F. Briesmeister, Los Alamos Report LA-12625-M Version 4B, 1997.
[5] W.R. Nelson et al., SLAC Report SLAC-265, 1985.
[6] I. Kawrakow et al., NRCC Report PIRS-701, 2003.
[7] R. Brun et al., GEANT3 Report DD/EE/84-1, 1986.
[8] S. Agostinelli et al., Nucl. Instr. Meth. A 506 (2003) 250–303.
[9] E.J. Williams, Proc. R. Soc. (London) A169 (1939) 531.
[10] G. Molière, Z. Naturforsch 3a (1948) 78.
[11] H.W. Lewis, Phys. Rev. 78 (1950) 526.

[12] S. Goudsmit et al., Phys. Rev. 57 (1940) 24.
[13] L. Urban, CERN-Open-2006-077, 2006.
[14] I. Kawrakow et al., Nucl. Instr. Meth. B 142 (1998) 253–280.
[15] F. Salvat et al., Comput. Phys. Commun. 165 (2005) 157–190.
[16] I. Kawrakow et al., Nucl. Instr. Meth. B 134 (1998) 325–336.
[17] A.F. Bielajew et al., Nucl. Instr. Meth. B 173 (2001) 332–343.
[18] E. Benedito et al., Nucl. Instr. Meth. B 174 (2001) 91–110.
[19] A.O. Hanson et al., Phys. Rev. 84 (4) (1951) 634–637.
[20] A.F. Bielajew et al., Nucl. Instr. Meth. B 86 (1994) 257–269.
[21] S.M. Seltzer et al., Nucl. Instr. Meth. 119 (1974) 157–179.
[22] O. Kadri et al., Nucl. Instr. Meth. B 258 (2007) 381–387.
[23] G.J. Lockwood et al., Sandia Report Sand79-0414.UC-34a, February 1987.